

Scientific session of the Division of General Physics and Astronomy of the Russian Academy of Sciences (28 February 2001)

A scientific session of the Division of General Physics and Astronomy of the Russian Academy of Sciences (RAS) was held on 28 February 2001 at the P L Kapitza Institute for Physical Problems, RAS. The following reports were presented in the session:

(1) **Novikov I D** (Astro Space Center, P N Lebedev Physical Institute, RAS, Moscow) “‘Big Bang’ echo (cosmic microwave background observations)”;

(2) **Karachentsev I D** (Special Astrophysical Observatory, RAS, Nizhniĭ Arkhyz, Karachaevo-Cherkessia, Russia) “‘Hidden mass in the Local Universe’”;

(3) **Cherepashchuk A M** (P K Sternberg Astronomical Institute, M V Lomonosov Moscow State University, Moscow) “‘Searches for black holes: the recent data’”;

(4) **Yakovlev D G** (A F Ioffe Physical Technical Institute, St.-Petersburg) “‘Superfluidity in neutron stars’”.

Summaries of the four papers are given below.

PACS numbers: 95.85.Bh, 98.80.Cq, 98.80.Es
DOI: 10.1070/PU2001v044n08ABEH000983

‘Big Bang’ echo (cosmic microwave background observations)

I D Novikov

The more than 60 successful projects on measuring the cosmic microwave background (CMB) anisotropy that have been carried out in the last 10 years have resulted in qualitative changes in observational cosmology. Starting from the pioneering papers [1–5], there has been steadily growing attention to this rapidly developing field of astrophysics. The importance and topicality of CMB anisotropy measurements are due to the unique possibility of obtaining ‘precision’ data on very important parameters of the modern Universe, such as the Hubble constant $H_0 = 100h \text{ km s}^{-1} \text{ Mpc}^{-1}$, the fraction of the baryon (Ω_b) and ‘hidden’ (dark) (Ω_m) mass, the cosmological constant Ω_Λ (all the quantities are in units of the critical density), the spectral index of pre-galactic inhomogeneities n_s , and some others.

The first successful results of this program were obtained by the COBE project [6], in which the CMB temperature fluctuations on the celestial sphere were first recorded at a level of $\Delta T/T \approx 10^{-5}$ at frequencies of 53 and 90 GHz with an angular resolution of $\text{FWHM} = 7^\circ$. The corresponding part of the spectrum of perturbations that give rise to the CMB anisotropy on angular scales $\theta > 7^\circ$ is related to spatial

fluctuations on scales $\lambda > 300 \text{ Mpc}$, which far exceed the typical size of the observed structures in the Universe. After COBE, special attention has been given to data obtained in ground-based, balloon, and space experiments, which provide a detailed signal structure with a higher angular resolution than that of COBE, down to $\text{FWHM} \approx 3'$.

Among them, such projects as Sascatoon, QMAP, MSAM, CBI, BOOMERANG, MAXIMA 1, etc. should be particularly noted (see [7] for a detailed description). Note that today the cosmological parameters have been determined with a record accuracy from the CMB anisotropy data obtained in the last two experiments (the corresponding errors in the anisotropy spectral characteristics do not exceed $\delta c_l/c_l = 10\%$ in the range of angles $0 \leq \theta < 1^\circ$).

On the whole, the data on the total density obtained by BOOMERANG and MAXIMA 1 are in good agreement with the inflation theory prediction that the present-day total density of all forms of matter should be close to the critical value: $\Omega_b + \Omega_m + \Omega_\Lambda = 1.09 \pm 0.07$ [8]. However, these data yield a relatively high baryon content, $\Omega_b h^2 = 0.031 \pm 0.005$, which exceeds the optimal value $\Omega_b h^2 \approx 0.02$ derived from the observed cosmic abundance of ^4He , deuterium, and hydrogen. Essentially, the analysis of the data of the MAXI–BOOM collaboration leads to the conclusion that the ‘standard’ $\Lambda + \text{CDM}$ cosmological model ($\Omega_m + \Omega_b + \Omega_\Lambda = 1$; $\Omega_b h^2 = 0.019$; $\Omega_m = 0.3$; $h = 0.65$, and $n_s = 1$) falls outside the data optimum at the 95% confidential level [8]. The models with 5–10% deviations from the Harrison–Zeldovich spectrum ($n_s \approx 1.05 \pm 0.09$) or with the recombination occurring at redshifts $Z \approx 10–15$ are preferable. However, as was shown in [9], the above modifications of the standard ΛCDM cosmology are characterized by virtually the same rms deviation $\chi^2 \approx 6.75–6.79$, including the model with ‘delayed’ recombination [9]. In practice, this means that it is impossible to make a choice between the models at the current accuracy level of discriminating the signal from noises of different origins. However, even with growing accuracy, the situation may change insignificantly, since, for example, the level of fluctuation suppression at small angles due to the ‘red’ spectral slope $n_s = 0.95$ and the level of fluctuation weakening due to the secondary ionization turn out to be very close. The above ‘degeneracy’ problem can be solved in two principal ways. First, in any case, it is necessary to increase the accuracy of the determination of the anisotropy spectrum both by increasing the sky coverage by observations (the so-called ‘cosmic variance problem’) and by decreasing the internal noise level of detectors. Second, it is of fundamental importance to measure the polarization fluctuations along with the CMB anisotropy. It is these two directions that will be realized both in the framework of the next launches of the MAXI–BOOM collaboration, and in the most promising space projects MAP and PLANCK. Note that, unlike the

already recorded CMB anisotropy, the polarization of radiation will be studied for the first time at the signal detection level. However, for polarization experiments, in which the signal-to-noise ratio does not exceed a few units (unlike the anisotropy, for which the signal-to-noise ratio is expected to be 10–30), of extreme importance are the methods of filtration of galactic and extragalactic noises related to the polarization properties of synchrotron and free-free emission, due to the dust radiation, contribution from point sources, etc. Of special importance for the future polarization experiments is taking into account the anisotropy that is introduced by the receiving tract and depends on the reception frequency due to the apparatus features of the experiment. In this connection, methods of data processing that are capable of maximum cleaning of noise from maps (rather than ‘spreading’ them over the power spectrum) should play a crucial role in the signal extraction. One such method involves an amplitude–phase analysis [10] based on removing noise not in the amplitude but in the phase space, where non-gaussian noise turns out to appear most significantly. An important role in the noise identification should be played by the method of singular points of the polarization field [11–13], which takes into account the fact that the signal structure in the zones without original polarization (‘singular points’) is determined by noise. The phase analysis of anisotropy and polarization maps is especially important to distinguish the contribution from the receiving tract (antenna + aberrations). By and large, the above methods of cleaning anisotropy and polarization maps will be an invaluable addition to such traditional methods as MEM (maximum entropy method), RC (radical compression), and wavelet analysis.

To conclude, we emphasize that in the next 10 years, undoubtedly, outstanding results will be obtained in experimental studies of the CMB anisotropy and polarization, which will naturally summarize almost half a century of CMB research. Looking into the future, we can say with certainty that the epoch of MAP and PLANCK projects will bring us plenty of bright important discoveries that will advance our understanding of the general laws (and details!) of the structure and evolution of the Universe.

References

1. Sakharov A D *Zh. Eksp. Teor. Fiz.* **49** 345 (1965) [*Sov. Phys. JETP* **22** 241 (1966)]
2. Silk J *Astrophys. J.* **151** 459 (1968)
3. Peebles P J E, Yu J T *Astrophys. J.* **162** 815 (1970)
4. Zel'dovich Ya B, Syunyaev R A *Astrophys. Space Sci.* **7** (1) 1 (1970)
5. Zel'dovich Ya B, Kurt V G, Syunyaev R A *Zh. Eksp. Teor. Fiz.* **55** 278 (1968) [*Sov. Phys. JETP* **28** 164 (1968)]
6. Bennet C L et al. *Astrophys. J. Lett.* **464** L1 (1996)
7. Hu W, <http://www.sns.ias.edu>
8. de Bernardis P et al. *Nature* **404** 955 (2000); Hanany S et al. *Astrophys. J.* **545** L5 (2000)
9. Naselsky P D et al., astro-ph/0102378
10. Naselsky P D, Novikov D I, Silk J, in *Proc. IA Symp. 201. Manchester, August 7–14, 2000*; astro-ph/0007133
11. Naselsky P D, Novikov D I *Astrophys. J.* **507** 31 (1998)
12. Dolgov A D et al. *Int. J. Mod. Phys. D* **8** 189 (1999)
13. Naselsky P et al., in *Proc. IA Symp. 201. Manchester, August 7–14, 2000*; astro-ph/0012319

PACS numbers: **95.35.+d**, **98.65.–r**

DOI: 10.1070/PU2001v044n08ABEH000969

Hidden mass in the Local Universe

I D Karachentsev

1. Brief history

The history of studies of hidden (dark, obscured) matter in the Universe traces back to 1933, when F Zwicky discovered [1] that masses tens of times higher than the sum of masses of individual galaxies are required to explain the observed velocities of galaxies in rich clusters. Later, the inconsistency between the ‘virial’ (based on the virial theorem) and individual masses was shown to be typical of galactic systems of different scales, from pairs and groups to clusters and superclusters of galaxies. In the 1970s, Freeman, Sancisi, and Rubin discovered that the rotational curves of many galaxies do not approach the Keplerian asymptotic at large distances from the centers but instead remain ‘flat’, which requires a substantial mass to be present at the outskirts of the galaxies [3]. Some authors believed that massive dark ‘coronae’ extend tens of times further than the visible boundaries of galaxies and that their total mass is capable of explaining the ‘virial paradox’ in clusters [4, 5]. In the 1980s, the X-ray emission of hot gas in galactic clusters with temperatures exactly corresponding to the virial motions of the galaxies was detected [6]. Finally, the most direct determinations of cluster masses from the gravitational lensing effect or shape distortions in the images of more distant galaxies [7] confirmed the presence of large unseen masses in rich clusters. It is firmly established that the estimates of rich cluster masses obtained using both virial motions and X-ray gas-emission properties and gravitational lensing effects agree within 50%.

However, such an agreement has not yet been reached on all scales of the Universe structural hierarchy. Table 1 lists the main mean characteristics of galactic systems of different scales, from single galaxies to clusters: the radius of the system, the root-mean-square velocity of the internal motions, the relative number of galaxies in the system at a given level, the total mass-to-luminosity ratio M_{\odot}/L_{\odot} , the mean dark-to-visible mass ratio (DM/LM), and the relative contribution of the galactic system to the total mass density in the Universe. Here the Hubble constant is taken to be $H = 70 \text{ km s}^{-1} \text{ Mpc}^{-1}$, which corresponds to the critical

Table 1. The dark matter distribution.

Properties	Galaxies	Pairs	Groups	Clusters
Radius, Mpc	0.03	0.09	0.25	1.7
R.m.s. velocity, km s^{-1}	(25)	35	70	600
Relative number of galaxies in the system	0.35	0.15	0.40	0.10
M_{\odot}/L_{\odot}	20	20	30–(200)	250
Method of estimation	Rotational curves	Orbital motions	Virial motions, sphere $V=0$	X-ray, grav. lensing
DM/LM	2	2	3–(27)	35
Specific contribution to the total mass	15 %	6 %	27 %	52 %
	(6 %)	(2 %)	(72 %)	(20 %)

density $\Omega_0 = 1.0 \times 10^{-29} \text{ g cm}^{-3}$. Within the standard optical radius, the visible-mass-to-luminosity ratio for a typical galaxy is about $7M_\odot/L_\odot$. For the mean luminosity density in the Universe $1.4 \times 10^8 L_\odot \text{ Mpc}^{-3}$ [5], the mean dark matter density is about 0.048–0.125 in units of the critical density.

The data presented here show that the intermediate hierarchical class, groups of galaxies, has the maximum difference in the hidden-mass estimates. Many authors find the mean virial-mass-to-luminosity ratio for groups to be $\sim 200M_\odot/L_\odot$ [8]. However, our data [9] indicate this ratio to be only $\sim 30M_\odot/L_\odot$. In the first case, groups of galaxies give the main contribution (72%) to the total density in the Universe, while in the second case the main contribution (52%) is provided by rich clusters. This also causes the uncertainties in the mean dark matter density determination in the Universe (from 0.048 to $0.125\Omega_0$). To clarify the situation, a detailed systematical study of the structure and dynamics of the closest groups of galaxies was required.

2. Topography of the Local Universe

As was stressed many times by J Peebles [10], precise knowledge of the distances and velocities of nearby galaxies allows one to calculate their mutual positions at different epochs Z and thus to determine the value of Ω_m at $\sim (1-10)$ Mpc scales. Unfortunately, until recent years the situation with radial velocities and, especially, with distances to galaxies in the Local Universe was discouragingly poor. For example, in a sample of $N = 179$ neighboring galaxies with radial velocities $V < 500 \text{ km s}^{-1}$ [11], reliable distances had been determined only for 8% of the galaxies. Moreover, recently strong arguments were put forward that the expected galactic number density in the Universe is an order (!) of magnitude higher than the observed one [12, 13]. It is assumed that not yet discovered galaxies are dwarf systems with a very low surface brightness and their contribution to the total mass is comparable with that from normal galaxies.

In recent years, at the Special Astrophysical Observatory (SAO) of the Russian Academy of Sciences, in cooperation with the Max-Planck-Institut (Germany) and other observatories in Spain, the USA, the Ukraine, and Finland, a program of searching for and investigation of new nearby galaxies has been carried out. The program includes the following stages.

(1) Searching for new nearby dwarf galaxies on the reproductions of the photographic sky survey POSS-II and ESO/ESRC. As a result, more than 600 nearby galaxy candidates were discovered.

(2) Measuring the radial velocities of the new galaxies using 21 cm neutral hydrogen line observations, with radio telescopes of Germany, France, and Australia, as well as using optical emission lines, with the 6-m telescope of the SAO RAS.

(3) Large-scale imaging of all close galaxies on the 6-m telescope and other telescopes with CCD detectors and resolving the galaxies into stars with an accuracy of $\sim 20\%$ using the luminosity of the brightest stars.

(4) Surveying the closest 200 galaxies using the Hubble Space Telescope, measuring their distances with an accuracy of $\sim 5\%$ from the luminosities of the red giant branch stars.

The main stages of this project have now been completed. The number of galaxies in the Local Volume, bounded by a distance of $D = 7 \text{ Mpc}$ or by radial velocities $V < 500 \text{ km s}^{-1}$, has been doubled. The number of galaxies with measured (photometric) distances has been increased by more than an

order of magnitude [14–16]. A unique stratum of new observational data has been obtained, which has allowed for the first time the reconstruction of a three-dimensional map of the Local Volume of the Universe and to study the peculiar velocity field inside it.

The relief of the Local Universe has a pronounced fractal structure with voids of different scales. Galaxies assemble into filamentary and planar structures surrounding the voids. Of the entire population of the Local Volume (340 galaxies), more than a half are concentrated in the attraction zone only of 7 of the most massive galaxies. These galaxy ‘oligarchs’ include, in particular, our Milky Way. The spatial crowding of galaxies is characterized by a two-point correlation function with a standard power law $\gamma = -1.8$. The standard Peebles correlation function describes the assembling of galaxies down to a scale comparable with the diameter of an individual galaxy (30 kpc).

3. Anisotropy of the velocity field of galaxies

The new data on the radial velocities and distances of 180 galaxies from the Local Volume reveal significant deviations from the isotropic Hubble expansion [16]. The observed distribution of the local Hubble parameter over the sky can be represented by a triaxial ellipsoid with an axis ratio $H_a : H_b : H_c = 81 : 62 : 48 \text{ km s}^{-1} \text{ Mpc}^{-1}$ to within an uncertainty of $\sim 8\%$. Minimum values of the Hubble parameter are observed along the polar axis of the Local Supercluster, and the region of maximum values lies along the Supercluster’s equator, at an angle of $\Theta = 29^\circ \pm 5^\circ$ with respect to the Virgo cluster center. By and large, the local pattern of the non-Hubble motion of galaxies has little correspondence with the well-known model of a spherically symmetric flow of galaxies towards the Virgo center [17]. One of the reasons for this discrepancy could be the differential rotation of the Local Supercluster. However, the existence of the large angular momentum on a $\sim 10 \text{ Mpc}$ scale is hard to understand in the framework of the modern cosmological models.

4. The Local Group and Hubble dependence in its surroundings

Our Galaxy (Milky Way) and the Andromeda galaxy (M31) together with 30 of their satellites form the Local Group. The volume distribution of the 70 closest galaxies inside and around the Local Group in a $\pm 3 \text{ Mpc}$ cube is shown in Fig. 1. For most of these galaxies, precise distance measurements have been carried out during the last two years. The two darker balls around the Andromeda galaxy indicate the two new satellites discovered at SAO in 1999 [18]. Figure 2 shows the radial velocity V_{LG} — distance D_{LG} relation for the nearest galaxies outside the Local Group. The Hubble dependence $V = HR$ relative to the Local Group centroid exhibits the expected non-linear effect due to the gravitational braking of the Hubble flow by the Local Group mass. The radius of the zero-velocity sphere R_0 and the total mass of the group are simply related as $M_{\text{LG}} = (\pi^2/8G)H^2 R_0^3$ [19], where G is the Newton gravity constant. For $H = 70 \text{ km s}^{-1} \text{ Mpc}^{-1}$ and the observed value $R_0 = 0.96 \pm 0.05 \text{ Mpc}$, the total mass of the Local Group is $(1.2 \pm 0.2) \times 10^{12} M_\odot$ and the mass-to-luminosity ratio is $M/L = (23 \pm 4) M_\odot/L_\odot$. Note that the obtained total mass agrees well with the sum of the mass of M31 $(0.8 \pm 0.4) \times 10^{12} M_\odot$ and that of the Milky Way $(0.9 \pm 0.4) \times 10^{12} M_\odot$, as estimated from the orbital motions of their satellites on the scale $\sim 200 \text{ kpc}$ [20, 21].

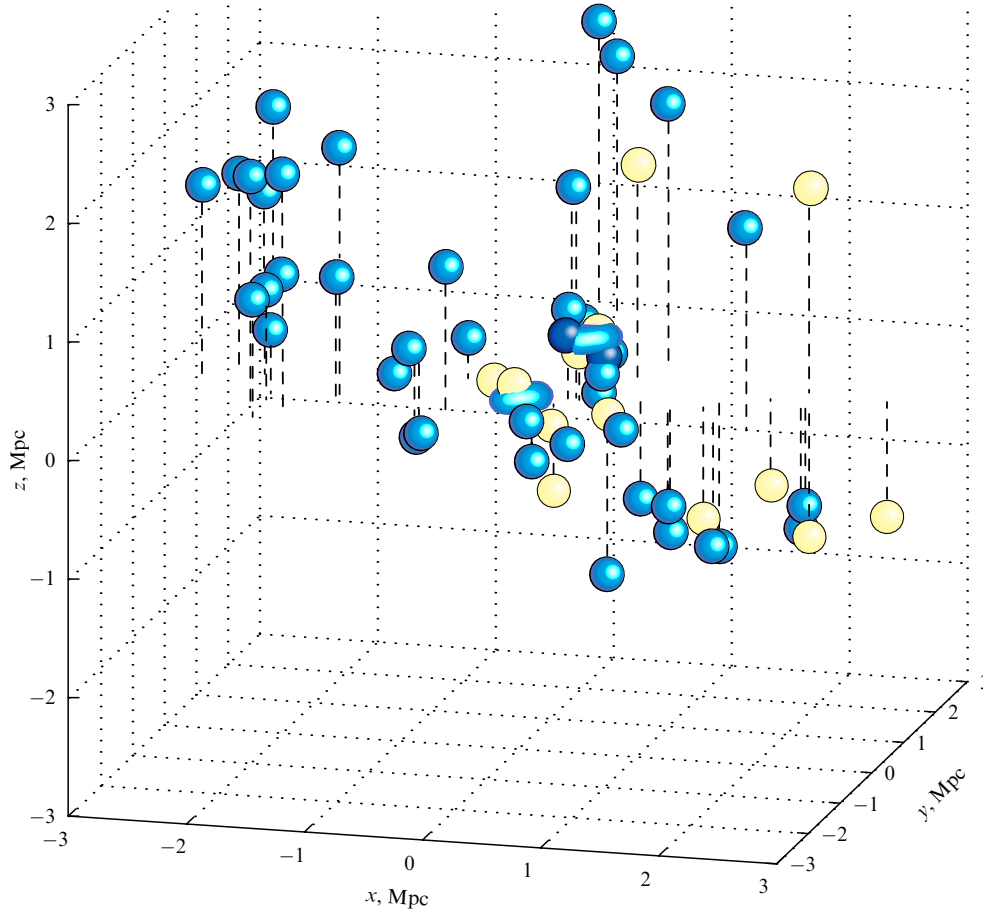


Figure 1. The Local group and its surroundings.

Most galaxies in Fig. 2 are well-isolated objects. Their radial-velocity variance with respect to the Hubble law is only 25 km s^{-1} , which can be considered the first reliable estimate of thermal (chaotic) galactic motions in the space between groups. With due account for the virial motions, the mean radial-velocity variance in the Local Volume is 72 km s^{-1} . According to [22], such a ‘cold’ field of peculiar velocities limits the mean local matter density to $\Omega_m < 0.08$.

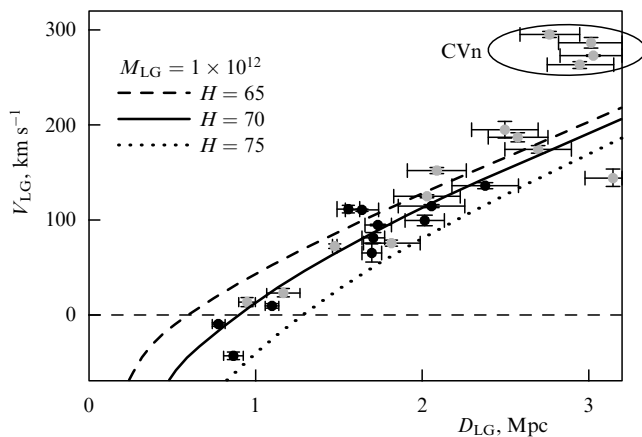


Figure 2. Velocities and distances of nearby galaxies relative to the centroid of the Local Group. The three lines (from left to right) correspond to the expected Hubble dependence for $H = 70 \text{ km s}^{-1} \text{ Mpc}^{-1}$ and values for the total mass of the Local Group of 3×10^{11} , 1×10^{12} and $3 \times 10^{12} M_\odot$. The oval marks four galaxies from the ‘cloud’ of Canes Venatici.

5. The nearby complex of galaxies M81

The group of galaxies nearest to us includes the spirals M81, NGC2403, NGC4236 and extends in the form of a filament over $\sim 30^\circ$. In view of the 12 recently discovered dwarf systems, the population of the complex amounts to 34 galaxies. Radial velocities have been measured for 23 of them, and distance determinations have been made for 28 of them using the Hubble Space Telescope with an accuracy of $\sim 200 \text{ kpc}$ [23]. From an analysis of the volume structure and kinematics of this complex, the zero-velocity sphere radius of the M81 group was determined to be 1.1 Mpc , which corresponds to a total mass of $1.8 \times 10^{12} M_\odot$ or a total-mass-to-luminosity ratio of $30 M_\odot/L_\odot$. The masses of galaxies M81 ($1.4 \times 10^{12} M_\odot$) and NGC 2403 ($0.4 \times 10^{12} M_\odot$) derived from the orbital motions of their satellites are in good agreement with the total group mass estimate. Therefore, both in the case of the Local Group and the M81 group, the total group mass (a scale of $\sim 1 \text{ Mpc}$) is consistent with the sum of orbital (virial) masses of the main galaxies in the subgroups (scales of $100\text{--}200 \text{ kpc}$). This implies that the main fraction of the volume of these groups is apparently not filled with dark matter.

6. Groups in the Local Supercluster

To single out groups of galaxies, simplified criteria [8, 24] have usually been applied, which ignore individual galactic properties. This has led to the contamination of groups with spurious members and a significant overestimation of the virial masses. Using more refined clusterization conditions [9, 25] notably reduced the mass estimates. The new criterion has

been applied to a sample of 6300 nearest galaxies with radial velocities $< 3000 \text{ km s}^{-1}$, concentrated within the Local Supercluster volume. As a result, 840 groups were selected that comprise 55% of the total number of galaxies in the volume. The typical characteristics of these groups are listed in Table 1. The mean crossing time of the groups does not exceed 10% of the Hubble time $1/H$. The mean virial-mass-to-luminosity ratio weakly depends on the group size and is $\sim 30 M_{\odot}/L_{\odot}$. The last value is consistent with the above total mass estimates for the Local Group and M81 group, which makes our system a typical representative of galactic groups.

7. Conclusion

A great number of possible candidates have been put forward to explain the nature of dark matter. They include: dwarf stars, black holes, molecular gas clouds, neutrinos, axions, gravitinos, etc.; see [26, 27] for reviews of various hypotheses and their observational tests. As can be seen from the last two rows of Table 1, the dark-to-visible mass ratio for single galaxies, pairs, and groups is $DM/LM = 2-3$, and only in rich clusters — dense ‘knots’ of the large-scale structure — this ratio increases by more than an order of magnitude. The total contribution of galaxies, pairs, and groups to the integral matter density ($15\% + 6\% + 27\%$) is approximately the same as that of rich clusters (52%). Possibly, we are observing two types of dark matter that have essentially different spatial distributions: compact, dark shells of individual galaxies and vast reservoirs filling the volumes of rich clusters.

It should be stressed here that there exist a strict relation between the luminosity of a galaxy and the amplitude of its internal motions (Tully – Fisher relation for spirals, Faber – Jackson relation for E and S0 galaxies), with a dispersion of only 15–20%. This means that unseen masses of galaxies are ‘sewed’ to their visible masses in a surprisingly stable proportion spanning a luminosity range of more than three orders of magnitude.

In recent years observational evidence has emerged [28] favoring the cosmological significance of vacuum, which appears as a universal repulsion force (the famous λ term in the Einstein equation). It cannot be ruled out that, in terms of vacuum cosmology, the problem of dark matter in the Universe will look essentially different.

References

1. Zwicky F *Helv. Phys. Acta* **6** 110 (1933)
2. Karachentsev I D *Astrofizika* **2** 81 (1966)
3. Freeman K C *Astrophys. J.* **160** 811 (1970)
4. Zaritsky D, White S D M *Astrophys. J.* **435** 599 (1994)
5. Bahcall N A, Lubin L M, Dorman V *Astrophys. J.* **447** L81 (1995)
6. Fabian A C et al. *Astrophys. J.* **248** 47 (1981)
7. Tyson J A et al. *Astrophys. J.* **281** L59 (1984)
8. Huchra J P, Geller M J *Astrophys. J.* **257** 423 (1982)
9. Makarov D I, Karachentsev I D *ASP Conf. Ser.* **209** 11 (2000)
10. Peebles P J E *Astrophys. J.* **449** 52 (1995)
11. Kraan-Korteweg R, Tammann G *Astron. Nachr.* **300** 181 (1979)
12. Klypin A A, Kravtsov A V, Valenzuela O *Astrophys. J.* **522** 82 (1999)
13. Bothun G, Impey C, McGaugh S *Publ. Astron. Soc. Pacific* **109** 745 (1997)
14. Karachentsev I D, Makarov D I *Astron. J.* **111** 535 (1996)
15. Karachentsev I D, Makarov D I, Huchtmeier W K *Astron. Astrophys. Suppl.* **139** 97 (1999)
16. Karachentsev I D, Makarov D I *Astrofizika* **44** 11 (2001)
17. Kraan-Korteweg R C *Astron. Astrophys. Suppl.* **66** 255 (1986)
18. Karachentsev I D, Karachentseva V E *Astron. Astrophys.* **341** 355 (1999)

19. Sandage A R *Astrophys. J.* **317** 557 (1987)
20. Evans N W, Wilkinson M I *Mon. Not. R. Astron. Soc.* **316** 929 (2000)
21. Zaritsky D et al. *Astrophys. J.* **478** 39 (1997)
22. Governato F et al. *New Astron.* **2** 91 (1997)
23. Karachentsev I D et al. *Astron. Astrophys.* **363** 117 (2000)
24. Maia M A G, Da Costa L N, Latham D W *Astrophys. J. Suppl.* **69** 809 (1989)
25. Karachentsev I *Astron. Astrophys. Trans.* **6** 1 (1994)
26. Trimble V *Ann. Rev. Astron. Astrophys.* **25** 425 (1987)
27. Weinberg D *ASP Conf. Ser.* **117** 578 (1997)
28. Perlmutter S et al. *Astrophys. J.* **517** 565 (1999)

PACS numbers: **04.70.**–S, 97.80.Jp, 98.35.Jk

DOI: 10.1070/PU2001v044n08ABEH000970

Searches for black holes: the recent data

A M Cherepashchuk

1. Introduction

Black holes are predicted by Einstein’s General Relativity (GR) theory. A black hole (BH) represents a space–time region for which the parabolic velocity is equal to the speed of light $c = 300\,000 \text{ km s}^{-1}$. The characteristic size of a BH is determined by the gravitational radius $r_g = 2GM/c^2$. It amounts to $r_g = 30 \text{ km}$ for $M = 10 M_{\odot}$ and 20 a.u. for $M = 10^9 M_{\odot}$. The BH event-horizon radius is $r_h = r_g$ for a non-rotating (Schwarzschild) BH and $r_h < r_g$ for a rotating one. For a BH that formed in our epoch, the event horizon has not yet formed, so these are collapsing objects (‘virtual’ BHs).

From the astronomical point of view, in order for an object to be recognized as a BH, its mass should be measured and its size should not exceed r_g . Also, it is necessary to obtain observational evidence for the object having a ‘virtual’ event horizon. BH masses are reliably measured by the surrounding gas and star motions. Since $r \gg r_g$, in most cases using the Newtonian gravity law is sufficient.

BH radii are very difficult to measure. So far only very rough ($r < 10r_g$) indirect estimates have been used: study of the X-ray luminosity due to accretion of matter onto a BH, fast time variability analysis, spectral line profile investigations, etc. No sufficient observational criteria for a BH have been found as yet, but all the necessary conditions are met.

There are 3 known types of BHs:

- (1) Stellar mass BHs with $M = 3-50 M_{\odot}$. The stellar evolution ends in the formation of a white dwarf (if the stellar core mass $M_c \leq 1.2 M_{\odot}$), a neutron star (NS) (if $M_c < 3 M_{\odot}$), or a BH (if $M_c \geq 3 M_{\odot}$).
- (2) Supermassive BHs in galactic nuclei ($M = 10^6 - 10^{10} M_{\odot}$).
- (3) Primordial BHs generated at the early stages of evolution of the Universe. As yet, very little is known about them from the observational point of view.

The existence of intermediate-mass BHs with $M = 10^2 - 10^4 M_{\odot}$ located in the near-nuclear regions of galaxies (at a mean distance of $\sim 390 \text{ pc}$ from the nucleus) has been widely discussed in recent years.

Observational studies of BHs proceed in two directions:

- (1) Searching for massive compact objects – BH candidates. Here much progress has been made, and the number of them approaches 100.
- (2) Looking for sufficient criteria for the BH candidates discovered to be real BHs. Many difficulties have been met on this avenue, but there is some progress and great hopes for future space X-ray, interferometric, and gravitational wave experiments.

2. Black hole mass determination

Galactic nuclei. In many cases, modern observational facilities allow direct measurements of gas and stellar motions around a BH (at distances $r \sim 10^4 - 10^5 r_g$). Therefore, the BH mass can be uniquely derived from the Newton gravity attraction law: $M_{\text{BH}} = rv^2/G$, where v is the velocity of the gas or stars, and r is the corresponding distance to the BH.

X-ray binary stars. In this case, the components are not separately visible, only the radial-velocity and light curves of the system can be measured. Assuming a point-like optical-star model and using the Newton gravity law, from the radial-velocity curve one can obtain the mass function of the optical star: $f_v(M) = M_x^3 \sin^3 i / (M_x + M_v)^2$, where M_x is the BH mass, and M_v is the optical star mass. The mass function $f_v(M)$ sets an absolute lower limit on the BH mass: $M_x > f_v(M)$. The effects of the optical star not being point-like, of its pear-like shape, and its X-ray heating-up are negligibly small for a mass ratio $q = M_x/M_v > 5$ (the case of transient X-ray binaries — X-ray novae). The BH mass can be expressed through the mass function: $M_x = f_v(M)[1 + (1/q)]^2(1/\sin^3 i)$. Since the components are not visible separately, there are two free parameters, q and i — the mass ratio and the inclination of the orbital plane of the binary system to the plane of the sky. The parameter i can be found from the analysis of the optical light curve of the system, which is mainly determined by the optical star ellipticity. The parameter q can be determined from the rotational broadening of absorption lines in the optical star spectrum (the star is not point-like and fills its Roche lobe). There are also some additional constraints allowing independent checks of the BH mass obtained from the mass function, such as data on X-ray eclipses, the distance to the system, the optical-star mass M_v estimated from its spectral class and luminosity class, and the orbital variability of absorption line profiles in the optical star spectrum.

3. Black hole radius determination

There are several means to determine the radius of a BH.

(1) From the X-ray luminosity and spectrum. The accretion X-ray energy release is $L_x = 0.057 \dot{M} c^2$ for a Schwarzschild BH and $L_x = 0.42 \dot{M} c^2$ for a Kerr BH. In X-ray binaries $L_x = 10^{36} - 10^{39} \text{ erg s}^{-1}$, which implies that the object is compact. However, the accretion rate \dot{M} is not known precisely. In addition, in the theory of advection-dominated accretion disks, L_x is small even for a known \dot{M} , since the main energy released in accretion is carried by hot ions, which rapidly disappear under the BH event horizon.

(2) From the minimal time scale Δt of the X-ray flux variability. For example, for Cyg X-1 $\Delta t = 10^{-3} \text{ s}$, $r < c\Delta t = 300 \text{ km} = 10 r_g$.

(3) From direct observations of BH surroundings in galactic nuclei using high-angular-resolution techniques. So far only weak restrictions are known: $r < 10^4 r_g$. The estimates will be improved in future with the use of space-based interferometers.

(4) From the width Δv of the FeXXV, FeXXVI emission line profiles at $\sim 6.4 \text{ keV}$: $\Delta v \approx 100\,000 \text{ km s}^{-1}$. The redshift of the broad line component corresponds to $r \sim 6 - 10 r_g$.

Additionally, in accordance with GR predictions, all known BH candidates of stellar masses do not exhibit X-ray-pulsar or type-I X-ray-burster phenomena, which are typical of accreting NSs. The spectral and time behavior of accreting NSs and BHs are systematically different.

4. Black hole masses in X-ray binaries.

At present, there are 15 known massive ($M_x > 3 M_\odot$) compact ($r < 10 r_g$) X-ray sources in close binary systems (BH candidates): $M_x = 4 - 15 M_\odot$. Among them, four reside in massive X-ray binaries with hot massive O–B or WR stars as secondary companions. These are systems Cyg X-1, LMC X-3, LMC X-1, and Cyg X-3. Eleven are known in transient X-ray binaries (X-ray novae), which have cold low-massive A–M stars as secondary companions. These include the systems AO620-00, GS2023+338, GRS1124-68, GS2000+25, GROJ0422+32, GROJ1655-40, H1705-250, 4U1543-47, GRS1009-45, SAXJ1819.3-2525, and XTE1118+480. No X-ray pulsars or type-I X-ray bursters, which would indicate an accreting NS, are found among them, in full agreement with GR predictions. The mean BH mass is $\bar{M}_x = 8 - 10 M_\odot$. The masses of 18 X-ray and radio pulsars and one type-I X-ray burster (all NSs) in binary systems, in accordance with GR, do not exceed $3 M_\odot$ and lie within narrow limits $M_{\text{NS}} = 1 - 2 M_\odot$.

The mass distribution of relativistic objects is bimodal: the mean NS mass is $\bar{M}_{\text{NS}} = (1.35 \pm 0.15) M_\odot$ and the mean BH mass is $\bar{M}_{\text{BH}} = 8 - 10 M_\odot$. Neither NS nor BH have been observed within the mass range $2 - 4 M_\odot$.

Wolf–Rayet (WR) stars are progenitors of relativistic objects in close binary systems. They are bared helium cores of massive stars that have lost their extended hydrogen envelopes in the course of the mass exchange in binary systems. Mass determinations have been made for 24 WR stars in WR+O systems. WR masses are distributed continuously over a broad interval $M_{\text{WR}} = 5 - 55 M_\odot$. With due account for radial stellar-wind mass losses, the masses M_{CO}^f of carbon-oxygen cores of WR stars at the end of their evolution can be calculated. They lie in a wide range, $M_{\text{CO}}^f = (1 - 2) - (20 - 44) M_\odot$, and are also continuously distributed. The mean value $M_{\text{CO}}^f = 7 - 10 M_\odot$ is close to the mean BH mass $\bar{M}_{\text{BH}} = 8 - 10 M_\odot$.

The difference in mass distributions of relativistic objects and CO cores of massive stars at the end of their evolution allows us to suppose that not only the pre-supernova mass determines the nature of the relativistic object (NS, BH), but also other pre-supernova parameters, such as rotation, magnetic field, etc., play a role. NSs and BHs in X-ray binaries differ not only in their masses but also in their observational appearances, as predicted by GR. This lends more credibility to our assurance that stellar-mass BHs really exist.

5. Black hole masses in galactic nuclei

Mass determinations have been made for more than 60 supermassive ($M > 10^6 M_\odot$), compact ($r < 10 r_g$), and in most cases dark (mass-to-luminosity ratio $M/L > 100$) bodies residing in galactic nuclei: $M = 10^6 - 10^{10} M_\odot$. About 20 masses of Active Galactic Nuclei were derived from the time retardation effect in rapidly varying emission lines with respect to the continuum (the so-called reverberation mapping method). The retardation times measured in different galaxies fall within the range $\Delta t = 5 - 80$ days. The distance from the BH to the emitting line gas clouds is $r = c\Delta t$. The characteristic velocity of the gas clouds motion \bar{v} can be determined from the Doppler line widths. Then the BH mass is $M = \eta \bar{v}^2 r / G = 10^7 - 10^8 M_\odot$, where the parameter $\eta = 1 - 3$ takes into account the character of motion of gas clouds around the BH ($\eta = 1$ for circular motions).

High angular resolution observations of the central regions (nuclei) of many galaxies (M87, NGC4621, NGC7052, etc.) made with the Hubble Space Telescope allowed measurements of the rotational velocity distribution of the central gas structures and mass determination of the underlying BH: $M = 10^8 - 10^9 M_\odot$.

Very-long-baseline interferometric observations (VLBI) of maser sources in near-nuclear regions permitted reliable BH-mass determinations in the case of NGC4258 ($M = 3.9 \times 10^7 M_\odot$) and in five other galaxies.

Measurements of the velocities and accelerations of individual stars near the center of our Galaxy allowed their orbits to be determined at distances $r < 0.005$ pc ($\cong 10^4 r_g$) from the central BH. Its mass, as derived from the distribution of individual star velocities in our Galaxy, is $2.6 \times 10^6 M_\odot$. An independent estimate, based on the accelerations of individual stars, yields a BH mass of $3 \times 10^6 M_\odot$.

The X-ray luminosity of the Galactic center is very low ($L_x = 10^{37}$ erg s $^{-1}$) and is $\sim 10^{-8}$ of the critical Eddington luminosity. Using data for ~ 45 galaxies, a correlation has been found between the mass of the galactic bulge and that of the central BH: $M_{\text{BH}} \cong (0.2\% - 0.5\%) M_{\text{bulge}}$.

In two cases (our Galaxy and galaxy NGC4258), the observed matter density inside the measured nuclear region of the galaxy ($r < 0.005$ pc $\cong 1.5 \times 10^{16}$ cm $\cong 10^4 r_g$ for $M = 10^6 M_\odot$) is $\rho > 10^{12} - 10^{13} M_\odot/\text{pc}^3 = 10^{-10} - 10^{-9}$ g cm $^{-3}$ (in the solar neighborhood $\rho \approx 0.1 M_\odot/\text{pc}^3$, in the most dense stellar clusters $\rho \sim 10^5 M_\odot/\text{pc}^3$). At $\rho > 10^{12} - 10^{13} M_\odot/\text{pc}^3$, the characteristic time scale of evaporation of individual dark bodies is $T_{\text{dyn}} < 10^8 - 10^7$ yr for galactic ages of $\sim 10^{10}$ yr. So massive dark bodies in the nuclei of our Galaxy and NGC4258 must be single compact objects.

The width and profile of the X-ray line FeXXV at 6.4 keV in the spectra of some galactic nuclei correspond to hot-gas ($T \cong 10^7$ K) velocities of $V_{\text{rot}} = 100\,000$ km s $^{-1}$ at distances of $r = (3-6) r_g$.

All these data strengthen our assurance of the existence of supermassive BH in galactic nuclei.

6. Prospects for finding sufficient criteria of BH existence

In future, the following experiments are envisaged which will provide sufficient criteria of BH existence.

(1) Space-based radio and X-ray interferometers with an angular resolution of $10^{-6} - 10^{-7}$ arcsec. These facilities will provide a possibility to directly observe processes near the event horizon, which has an angular size of $\sim 10^{-6}$ arcsec in nearby galactic nuclei.

(2) Gravitational wave bursts from binary BH mergings.

(3) Detection of a radio pulsar in a binary system with a BH (one pulsar in pair with a BH is expected per ~ 1000 single pulsars).

(4) Detailed studies of X-ray line profiles and rapid variability of X-ray fluxes from accreting BHs.

(5) Studying the gravitational microlensing of galactic nuclei by stars in intervening galaxies — gravitational lenses (angular resolution of up to 10^{-6} arcsec).

(6) Routine accumulation of reliable mass estimations of BH candidates and statistical comparisons of the observed NS and BH properties.

PACS numbers: 47.37.+q, 97.60.Gb, 97.60.Jd

DOI: 10.1070/PU2001v044n08ABEH000984

Superfluidity in neutron stars

D G Yakovlev

1. Introduction

Neutron stars (NSs) are the most compact of all stars. Their masses are around $1.4 M_\odot$, where M_\odot is the solar mass, and their radii are about 10 km. Accordingly, the mean density of the NS matter is a few times ρ_0 , where $\rho_0 = 2.8 \times 10^{14}$ g cm $^{-3}$ is the density of the matter in atomic nuclei. Atomic nuclei are almost incompressible in laboratory conditions. NSs are often called natural laboratories of supranuclear-density matter.

According to current views [1], a NS consists of four main layers. The outer layer, which extends to a density of 4×10^{11} g cm $^{-3}$, is the *outer crust*, which consists of degenerate electrons (e) and ions (nuclei). Deeper, to $\sim 0.5 \rho_0$, there is the *inner crust*, composed of nuclei, electrons, and free neutrons (n). Further, to $\sim 2 \rho_0$, there is the *outer core* containing a Fermi liquid of neutrons with a small admixture of degenerate electrons and protons (p) and, possibly, muons. Finally, the NS central region constitutes the *inner core*, whose composition is largely unknown. A reliable theory of the superdense NS matter is still absent. The main difficulty is in the description of strong interactions of various particles accounting for many-body effects. Instead of a strict theory, there are many different theoretical models. Some models predict the appearance of hyperons in the NS cores, while others predict either pion or kaon condensation or the appearance of light, almost free quarks (u, d, and s). One cannot exclude mixtures of different phases, for instance, hyperons and quarks. Some models give a fairly stiff equation of state and, therefore, rather high maximum allowed masses of NSs, $(2-3) M_\odot$. According to other theories, the equation of state is moderate or soft, and the maximum masses are lower, $(1.5-2) M_\odot$. The nature of matter in the NS cores is the main mystery of NSs. Its solution would be of fundamental importance for physics and astrophysics.

Let us mention a hypothesis of Witten [2], according to which a plasma of almost free quarks is the most stable state of matter not only at high pressures but also at zero pressure. If so, instead of NSs, so-called *strange stars* should exist, almost fully composed of quark matter of density $\gtrsim \rho_0$.

NSs are observed in all ranges of the electromagnetic spectrum, from radio to hard gamma rays. They may be either isolated objects or components of binary systems. They manifest themselves as radio and X-ray pulsars, X-ray bursters, X-ray transients, soft-gamma repeaters, or anomalous X-ray pulsars. The birth of NSs in supernova explosions leads to powerful neutrino outbursts. NSs may be powerful sources of gravitational radiation.

2. Superfluid gaps

One of the main features of NSs is *superfluidity* of the baryon component of their matter. It is believed that superfluidity is produced by Cooper pairing of baryons with opposite momenta under the action of the attractive part of the strong interaction of particles. Superfluidity is switched on as the temperature T falls below a critical temperature, T_c , leading to the appearance of a gap Δ in the baryon dispersion relation near the Fermi level. The gap

has practically no effect on the equation of state of matter, i.e., on the NS masses and radii.

One can expect superfluidity of free neutrons and superfluidity of nucleons in atomic nuclei in the inner NS crust. The superfluidity of n , p , and other particles is possible in an NS core. The superfluidity of charged particles, for instance, p , means superconductivity.

The superfluidity of neutrons in NSs was predicted by Migdal [3]. Wolf [4] showed, that singlet-state (1S_0) pairing of neutrons can occur in the NS crust but disappears in the NS core because the nuclear attraction of n in the singlet state turns into repulsion with increasing density. However, as pointed out by Hoffberg et al. [5], one can expect triplet-state (3P_2) pairing of n with an anisotropic gap in the NS core. Owing to a rather low fraction of p in the NS core, their pairing usually occurs in the singlet state. The critical temperatures T_{cn} and T_{cp} in NSs have been calculated by many authors (see, e.g., [6] for references). The results are sensitive to the nuclear interaction model and many-body theory employed; they are affected by kaon or pion condensations.

There may be pairing of hyperons [8] in hyperonic matter and pairing of quarks [9] in quark matter.

In all the cases mentioned above, microscopic calculations give critical temperatures $T_c \lesssim 10^{10}$ K and lower. Recently, a new type of quark superfluidity was proposed [9], which consists in pairing of unlike quarks (ud , us , ds). For a typical Fermi energy of quarks of ~ 500 MeV, one can expect critical temperatures of $T_c \sim 50$ MeV $\sim 5 \times 10^{11}$ K. However, this pairing is suppressed by the difference in the Fermi momenta of unlike quarks. If the difference is large enough, the pairing should disappear.

3. Vortices and fluxoids

For simplicity, consider first the core of a rotating NS composed of n , p , and e . The rotation of a neutron superfluid is realized [10,11] in the form of quantized vortices (Feynman-Onsager vortices) parallel to the NS spin axis. The total number of vortices in a NS is $\sim 2 \times 10^{16}/P$, where P is the spin period in seconds. The overall vortex motion of the neutron superfluid reproduces a solid-body rotation with the period P . The vortices also penetrate into the inner NS crust, where the superfluidity of n is present. The slowing-down of the neutron superfluid, which accompanies the NS spin-down, is associated with the outward drift of vortices and their disappearance at the boundary of the superfluid region.

Superconductivity of p in the NS core is described by the Ginzburg–Landau theory. The proton coherence length (2–6 fm) is typically much smaller than the London screening length (100–300 fm), i.e., a type-II superconductor forms. If the NS core initially contained a quasi-uniform magnetic field B , then after the superconducting transition this field splits into fluxoids (Abrikosov vortices), thin magnetic flux tubes parallel to the initial field. The total number of fluxoids is $\sim 10^{31} (B/10^{12} \text{ G})$.

Neutron vortices may be pinned by atomic nuclei or by defects of the crystal of atomic nuclei in the NS crust and also by fluxoids in the NS core. The pinning may be accompanied by vortex-creep effects. Owing to the drag of proton superfluid by neutron vortices (similar to the drag of superfluid ^3He by the motion of superfluid ^4He [12]), neutron vortices in the NS core acquire magnetic moments. Electrons (which are non-superfluid) scatter off

the magnetic fields of fluxoids and vortices [13], producing a strong coupling of electrons with superfluid n and p (so-called *mutual friction*). Vortices and fluxoids are also exposed to other forces (the Magnus force, buoyancy force etc.).

The superconductivity of quark matter is of a different character. According to estimates, a type-I superconductor forms in the case of any pairing of quarks (like or unlike). This superconductor expels the magnetic field (see Section 5).

4. Pulsar glitches

Isolated radio pulsars spin down slowly, transforming their rotational energy into electromagnetic radiation. Some pulsars show glitches. Within a very short time interval (probably, several minutes) the NS spin period decreases and then increases smoothly (relaxes), returning to the regime of slow permanent growth (NS spin-down) within a month or so. The most frequent and powerful glitches are exhibited by the Vela and Crab pulsars. The relative jumps of their periods are $\sim 10^{-6}$ and $\sim 10^{-8} - 10^{-7}$, respectively.

The most popular model of glitches was developed by Alpar et al. (e.g., [14]) and exploited the idea of n superfluidity. Owing to mutual friction (see Section 3), the pulsar core rotates almost as a rigid body. It is connected tightly with the non-superfluid part of the crust and rotates together with it. Only the n superfluid in the pulsar crust is relatively independent. The spin-down torque acts on the non-superfluid part of the crust. In the regime of persistent spin-down, the rotation of the n superfluid in the crust adjusts to the spin-down of the other part of the NS by means of the permanent unpinning of vortices from some pinning centers and pinning them to others. However, the lag of the spin-down of the neutron superfluid in the crust can be accumulated, leading finally to a glitch — the unpinning of numerous vortices at once and subsequent relaxation (pinning to new centers). The theory requires the moment of inertia of the neutron superfluid in the crust to be $\sim 10^{-2}$ of the total moment of inertia. The pinning of vortices in the pulsar core is difficult to calculate, which introduces great uncertainties into the theory.

5. Magnetic field evolution in an NS core

The core of a newly born NS may possess a strong magnetic field. First we describe its evolution in a model of the core composed of n , p , and e .

If superfluidity is absent then the magnetic field experiences normal ohmic decay. In a rather weak field ($B \lesssim 10^{11}$ G), the electrical resistance is isotropic and so weak that the decay time exceeds the age of the Universe [11]. In a stronger field, the resistance across the field may substantially increase owing to magnetization of e and p , which accelerates the decay to $10^6 - 10^8$ yr [15].

In the presence of (type-II) proton superconductivity the magnetic field evolution is determined by the drift of fluxoids. Simple estimates yield the typical time of fluxoid expulsion from a superconductor by ohmic diffusion $\sim 10^8$ yr [11]. Subsequent works took into account other mechanisms of interaction of fluxoids with the medium. These mechanisms have not been studied in full detail; the inclusion of all mechanisms together is a complicated task, and the results are not definite. For instance, Srinivasan et al. [16] took into account the interpinning of fluxoids and vortices. Vortices drift outwards following the pulsar spin-down and drag fluxoids, i.e., the fluxoid expulsion operates on spin-down time scales ($\sim 10^8 - 10^{10}$ yr). Ding et al. [17] included the

consideration of creep of fluxoids and vortices, as well as mutual friction. Hsu [18] incorporated the force that acts on fluxoids, being proportional to the gradient of the proton superfluid gap. In his model, fluxoids can drift to the NS center in the central region of the NS.

In a star with a superconducting quark core (type-I superconductor) the magnetic field is completely expelled from the core by the Meissner effect. Simple estimates [19] yielded the time of expulsion due to ohmic diffusion $\sim 10^4$ yr. Chau [20] noted that the expulsion may be accompanied by the enhancement of magnetic-field nonuniformities and prolonged to 10^7 yr. Alford et al. [21] considered an expulsion due to pairing of like and unlike quarks and obtained expulsion times larger than the age of the Universe in both cases.

The evolution of magnetic fields in NS cores requires further consideration. It may be coupled to the thermal evolution of NSs, evolution of the magnetic field in their crusts, and to the possible accretion of matter from the companion to the NS in a binary system.

6. Damping of stellar pulsations

NS pulsations can be generated by different mechanisms. Of particular interest are the so-called r-modes [22], associated with density waves, which are capable of emitting gravitational radiation and growing under the action of this radiation. It is assumed that the r-modes are generated in young rapidly rotating NSs born in supernova outbursts and live for a sufficiently long time (from several days to about one year), slowing down NS rotation and producing powerful gravitational radiation. Gravitational detectors of the new generation, e.g., LIGO II and LIGO III, could detect several such events per year from a distance of up to 20 Mpc.

However, pulsations can be damped by the viscosity of the matter in the NS core. In the absence of superfluidity, the typical damping time controlled by shear viscosity is $\tau \sim 10 T_9^2$ yr, where T_9 is the internal temperature expressed in 10^9 K. In a hot, non-superfluid NS the damping due to bulk viscosity appears to be stronger. Here, three cases can be distinguished.

(1) If the NS core contains neither hyperons nor quarks, and beta equilibrium is supported by modified Urca processes, then the damping of pulsations with frequency $\omega \sim 10^4$ s $^{-1}$ due to bulk viscosity [23] dominates at $T \gtrsim 10^9$ K and yields $\tau \sim 10/T_9^6$ yr. For a typical value $T \sim 10^9$ K, the time scale τ may be several years.

(2) If beta equilibrium is realized through direct Urca process, the bulk viscosity and neutrino cooling rate will be enhanced by several orders of magnitude [24]. The bulk viscosity will dominate at $T \gtrsim 10^8$ K, giving $\tau \sim 1/T_9^4$ min. In this case the temperature will decrease to $\sim 10^8$ K within several days, and τ will also be several days.

(3) In the presence of hyperons or quarks, the bulk viscosity is determined by neutrinoless reactions involving these particles [25, 26] and will be so high as to be able to dominate at $T \gtrsim 10^7$ K, giving $\tau \sim 1/T_9^2$ s.

Regardless of the neutrino cooling rate, we will have τ of a few minutes for a young and hot star. Thus, the existence of r-modes is critically sensitive to the presence of hyperons or quarks.

The effect of superfluidity on pulsation damping is twofold. On the one hand, the gap in the dispersion relation of superfluid particles can strongly suppress bulk viscosity and slow down the damping of pulsations [27]. On

the other hand, mutual friction is equivalent to a large effective viscosity, so that $\tau \lesssim 10^4$ s [28]. The onset of superfluidity in a cooling NS depends on the cooling regime and the values of T_c . It is possible that a young and hot NS remains non-superfluid and r-modes be unaffected by superfluidity. Even so, superfluidity may strongly damp pulsations of older NSs.

7. Neutron star cooling

The decrease of surface temperature in time in a cooling NS is governed, in particular, by the NS neutrino luminosity and heat capacity (see, e.g., [6]). The presence of the gap in the dispersion relation of superfluid particles affects the heat capacity and suppresses neutrino reactions involving these particles. Moreover, a new specific mechanism of neutrino emission appears due to Cooper pairing of particles. In the absence of superfluidity, we have either the so-called *slow* cooling, controlled by neutrino reactions of modified Urca process, or *fast* cooling due to direct Urca process. Superfluidity may affect the cooling process in such a way that fast cooling will look like slow cooling, and vice versa. Thus, superfluidity in the NS core may become a powerful cooling regulator. This allows one, in principle, to determine the critical temperatures in the NS cores by comparing cooling theories with observations of thermal radiation from NSs.

In particular, this has been done [6] for simplified models of NSs whose cores consist only of n, p, and e, assuming the critical temperatures T_{cn} and T_{cp} to be constant over the core. We have chosen NS models with masses 1.3 or $1.48 M_\odot$ corresponding to the turned-off and turned-on direct Urca process. The results have been compared with the surface temperatures of several middle-aged NSs (10^4 – 10^6 yr), inferred using the interpretation of the observed spectra with the black-body spectrum or hydrogen-atmosphere models. In all the four cases (two masses and two spectral models) we have determined the values T_{cn} and T_{cp} , which agree with the majority of observational data. In all the cases, we have obtained $T_{cn} \approx 3 \times 10^8$ K. These results are preliminary. At the next stage, more realistic models of superfluidity should be considered, with T_c variable over the NS core.

8. Summary

Superfluidity of the baryon component of matter (nucleons, hyperons, quarks) in NSs is predicted by almost all microscopic theories. However, the theoretical values of T_c are very uncertain.

Superfluidity strongly affects many processes in NSs (glitches, magnetic field evolution, pulsation damping, cooling); however, theoretical description of many superfluid effects is still far from perfect.

In principle, superfluidity can be studied by confronting theoretical models with observations of NSs. One can expect that these studies will clarify the properties of superfluidity and help in resolving the main mystery of NSs, i.e. in determining the composition and equation of state of matter in their cores.

This work is partly supported by the RFBR grant 99-02-18099.

References

1. Shapiro S L, Teukolsky S A *Black Holes, White Dwarfs, and Neutron Stars* (New York: John Wiley & Sons, 1983) [Translated into Russian (Moscow: Mir, 1985)]
2. Witten E *Phys. Rev. D* **30** 272 (1984)

3. Migdal A B *Nucl. Phys.* **13** 655 (1959)
4. Wolf R A *Astrophys. J.* **145** 834 (1966)
5. Hoffberg M et al. *Phys. Rev. Lett.* **24** 775 (1970)
6. Yakovlev D G, Levenfish K P, Shibano Yu A *Usp. Fiz. Nauk* **169** 825 (1999) [*Phys. Usp.* **42** 737 (1999)]
7. Balberg S, Barnea N *Phys. Rev. C* **57** 409 (1998)
8. Bailin D, Love A *Phys. Rep.* **107** 325 (1984)
9. Alford M, Rajagopal K, Wilczek F *Phys. Lett. B* **422** 247 (1998)
10. Ginzburg V L, Kirzhnits D A *Zh. Eksp. Teor. Fiz.* **47** 2006 (1964) [*Sov. Phys. JETP* **20** 1346 (1965)]
11. Baym G, Pethick C, Pines D *Nature* **224** 673 (1969)
12. Andreev A F, Bashkin E P *Zh. Eksp. Teor. Fiz.* **69** 319 (1975) [*Sov. Phys. JETP* **42** 164 (1976)]
13. Alpar M A, Langer S A, Sauls J A *Astrophys. J.* **282** 533 (1984)
14. Alpar M A, in *The Lives of the Neutron Stars* (Eds M A Alpar et al.) (Dordrecht: Kluwer, 1995) p. 185
15. Haensel P, Urpin V A, Yakovlev D G *Astron. Astrophys.* **229** 133 (1990)
16. Srinivasan G et al. *Current Sci.* **59** 31 (1990)
17. Ding K Y, Cheng K S, Chau H F *Astrophys. J.* **408** 167 (1993)
18. Hsu S D H *Phys. Lett. B* **469** 161 (1999)
19. Bailin B, Love A *Nucl. Phys. B* **205** 119 (1982)
20. Chau H F *Astrophys. J.* **479** 886 (1997)
21. Alford M, Berges J, Rajagopal K *Nucl. Phys. B* **571** 269 (2000)
22. Andersson N, Kokkotas K D *Int. J. Mod. Phys. D* **10** 381 (2001); gr-qc/0010102
23. Sawyer R F *Phys. Rev. D* **39** 3804 (1989)
24. Haensel P, Schaeffer R *Phys. Rev. D* **45** 4708 (1992)
25. Jones P B *Proc. Roy. Soc. London A* **323** 111 (1971)
26. Madsen J *Phys. Rev. D* **46** 3290 (1992)
27. Haensel P, Levenfish K P, Yakovlev D G *Astron. Astrophys.* **357** 1157 (2000)
28. Lindblom L, Mendell G *Phys. Rev. D* **61** 104003 (2000)